

Fluorescence Molecular Tomography Of Small Animals Using The Radiative Transfer Equation For Curved Geometries

Alexander D. Klose and Andreas H. Hielscher

*Departments of Biomedical Engineering & Radiology, Columbia University
MC 8904, 500 West 120th Street, New York, NY 10027, USA
Email: ak2083@columbia.edu*

Abstract: We have developed a fluorescence image reconstruction algorithm for three-dimensional whole-body small animal imaging. Our method uses non-contact fluorescent light measurement data on the tissue surface of the animal and reconstructs the three-dimensional unknown fluorophore concentration inside the tissue. The image reconstruction technique employs a light propagation model based on the equation of radiative transfer, which is solved on a structured Cartesian grid by a finite-difference method. A blocking-off approach takes the curved tissue surface geometry of the animal into account. Our proposed method has the advantage that fast numerical solvers for the equation of radiative transfer can be used.

© 2005 Optical Society of America

OCIS codes: (170.3010) image reconstruction techniques, (170.3660) light propagation in tissue, (170.5280) photon migration, (170.6960) tomography, (100.3190) inverse problems.

1 Introduction

Fluorescence molecular tomography (FMT) has emerged in recent years as a novel small imaging modality [1]. A fluorescent biochemical marker is injected into a small animal and will emit near-infrared light upon excitation by an external light source. From measurements of the light intensity on the tissue surface one seeks to determine the spatial concentration distribution of the marker inside the tissue. Since the fluorescent signal is proportional to the fluorophore uptake in tissue, the molecular probe concentration can be derived. We have recently presented the first transport-theory-based, three-dimensional, tomographic reconstruction algorithm for FMT [2, 3, 4]. The forward model based on the equation of radiative transfer (ERT) was defined on a structured *Cartesian* grid, but did not take curved geometries into account. Therefore, the small animal needed to be immersed into a cubic container with matching fluid to obtain simple geometries for modeling the light propagation. In the work presented here, we have extended our code to allow for non-contact measurement data as input. This has the advantage, optical tomographic images can be obtained from animals that are directly imaged with a CCD camera without immersing the animal into matching fluid. We show first numerical results of our new technique for reconstructing the unknown fluorophore distribution in a numerical mouse model.

2 Method

Our fluorescence image reconstruction method consists of two parts. First, a forward model for light transport based on the ERT predicts the detector readings (J^m) at emission wavelength λ^m on the tissue boundary for a given initial source distribution ($[S^m]^0 \sim [\mu_a^{fl}]^0$). Second, an inverse model is used to determine a new fluorophore distribution ($[\mu_a^{fl}]^i$) inside the medium. An objective function (φ) as part of that inverse model is defined, which is the χ^2 -error norm of the predicted partial current (J^m) and measured (M^m) detector readings. An updating scheme is used to iteratively modify the initial distribution along a search direction and determines the new fluorophore absorption coefficient (μ_a^{fl}) distribution inside the medium. The search direction is provided by the derivative of the objective function with respect to the present source distribution. The optimization process is finished after the measured and predicted data match and a minimum of the objective function is found. The final source distribution is displayed in an image.

The light distribution originating from internal fluorescent sources can be described by a hierarchical system of two ERTs for the radiance $\psi(\mathbf{r}, \boldsymbol{\Omega})$. First, an external light source S^x at the wavelength λ^x causes a fluence

distribution

$$\phi^x(\mathbf{r}) = \int_{4\pi} \psi^x(\mathbf{r}, \boldsymbol{\Omega}) d\boldsymbol{\Omega} \quad (1)$$

inside tissue that is calculated by the ERT

$$\boldsymbol{\Omega} \cdot \nabla \psi^x + (\mu_a^x + \mu_a^{fl} + \mu_s^x) \psi^x = \mu_s^x \int_{4\pi} p(\boldsymbol{\Omega}, \boldsymbol{\Omega}') \psi^x(\boldsymbol{\Omega}') d\boldsymbol{\Omega}' \quad (2)$$

with the scattering coefficient $\mu_s^x(\mathbf{r})$ and intrinsic absorption coefficient $\mu_a^x(\mathbf{r})$ at the wavelength λ^x . The total absorption consists of the intrinsic absorption $\mu_a^x(\mathbf{r})$ of the tissue and the absorption $\mu_a^{fl}(\mathbf{r})$ due to the fluorochrome. The fluorophore absorption $\mu_a^{fl}(\mathbf{r}) = c(\mathbf{r}) \cdot \epsilon$ is linearly proportional to the fluorophore concentration $c(\mathbf{r})$ and the fluorophore extinction coefficient ϵ .

Second, the fluence distribution $\phi^x(\mathbf{r})$ excites a fluorochrome inside the tissue at position \mathbf{r} . The excited fluorophore with the quantum yield η constitutes an internal source $S^m(\mathbf{r}, \boldsymbol{\Omega}) = \frac{1}{4\pi} \eta \mu_a^{fl}(\mathbf{r}) \phi^x(\mathbf{r})$ and emits light at the fluorescence wavelength λ^m . This fluorescent source is isotropic, and its strength depends linearly on the excitation field $\phi^x(\mathbf{r})$. The fluence distribution $\phi^m(\mathbf{r})$ of the fluorescent field is calculated by a second ERT [Equation (3)] with the optical parameters $\mu_a^m(\mathbf{r})$ and $\mu_s^m(\mathbf{r})$ at the fluorescence wavelength λ^m :

$$\boldsymbol{\Omega} \cdot \nabla \psi^m + (\mu_a^m + \mu_s^m) \psi^m = \frac{1}{4\pi} \eta \mu_a^{fl} \phi^x + \mu_s^m \int_{4\pi} p(\boldsymbol{\Omega}, \boldsymbol{\Omega}') \psi^m(\boldsymbol{\Omega}') d\boldsymbol{\Omega}'. \quad (3)$$

The predicted detector readings at the emission wavelength λ^m on the boundary at detector position \mathbf{r}_d are given by the partial current J^m . Both transport equations, Equations (2) and (3), are solved numerically with a finite-difference discrete-ordinates method. Furthermore, we are using a *blocking-off region* method for taking curved tissue geometries into account. In this approach the physical domain is modeled using a so-called *nominal domain*. A nominal domain is divided into two regions. First, the active region is that part of the physical domain where the solution is sought. Second, the inactive region lies outside the physical boundary, hence, all Cartesian grid points are blocked-off.

The spatial distribution of the fluorophore absorption, $\mu_a^{fl}(\mathbf{r})$, is reconstructed by minimizing an objective function $\Phi(\mu_a^{fl})$ with a Broyden-Fletcher-Goldfarb-Shanno (BFGS) method. The objective function describes the difference between the measured, M_d^m , and predicted data, J_d^m , for all D source-detector pairs

$$\Phi(\mu_a^{fl}) \approx \sum_{d=1}^D \left(\frac{J_d^m - M_d^m}{\sigma} \right)^2. \quad (4)$$

The predicted detector readings at the emission wavelength, λ^m , are calculated by Equation (3), whereas the excitation field at λ^x is determined by Equation (2).

3 Numerical results

A numerical mouse model was generated from a complete MRI data set consisting of 91 slices. The MRI slices were segmented and merged obtaining a three-dimensional numerical mouse model. This model consisted of 81,000 voxels that filled a volume of 1.9 cm \times 1.56 cm \times 5.4 cm. Each voxel inside the mouse volume was assigned the optical tissue parameters $\mu_s = 5 \text{ cm}^{-1}$ and $\mu_a = 0.4 \text{ cm}^{-1}$. Furthermore, the normal vector of all surface points of the mouse model was determined. A fluorescent source mimicking a molecular target (size: 0.2 \times 0.2 \times 0.2 cm³) was added to the numerical mouse model.

Twelve source points were placed around the circumference of the mouse as depicted by the red dots in Figure 1(a). These source points sequentially delivered an inward-directed light beam on the mouse surface. Furthermore, 504 detector points surrounded the mouse, see blue dots in Figure 1(a). These detector points constitute the positions where light escapes the tissue surface along the outward-direction. The light intensity could be measured, for example, with a CCD camera. The angle between the normal vector on the tissue

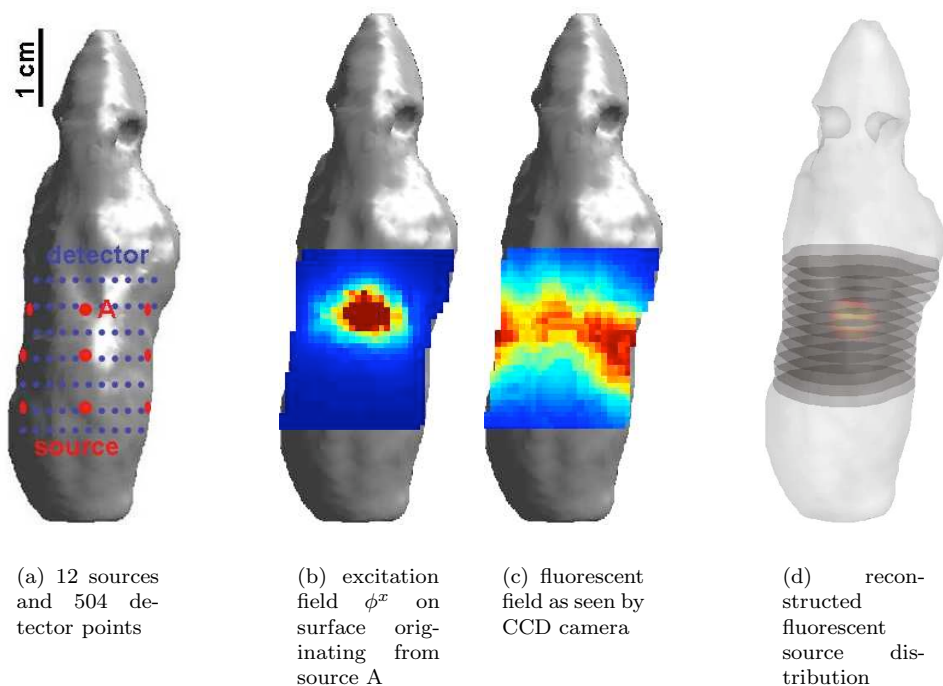


Fig. 1. Three-dimensional numerical mouse model containing a fluorescent target.

surface of the escaping light and the camera was taken into account. Each source point was assigned to 119 detector points, mostly on the side opposite the detector positions. Detector points in the proximity of the source positions were not used. Synthetic measurement data were generated knowing the exact molecular target position. The measurement data became input to the reconstruction algorithm and a three-dimensional fluorophore distribution was calculated. The reconstruction time was 40 hours.

The excitation source, which excites the fluorophore prior to emission, was placed at point (A) in Figure 1(a). Figure 1(c) depicts the fluorescent light intensity on the tissue surface originating from the molecular target, which was excited by source A. Figure 1(c) is usually seen by a CCD camera. Information about the position and strength of the fluorescent molecular target can not be obtained from a single CCD camera image. However, single CCD camera images are the common imaging procedure in direct fluorescent molecular imaging. On the other hand, a tomographic reconstruction as shown in Figure 1(d) displays directly the fluorescent source distribution. The position and the strength of the fluorescent source can easily be seen. A map of molecular probe concentration c can directly be derived from the reconstructed fluorophore absorption coefficient (μ_a^{fl}).

References

1. R. Weissleder, U. Mahmood, "Molecular imaging," *Radiology* 219, 316 (2001).
2. A.D. Klose, V. Ntziachristos, A.H. Hielscher, "In vivo fluorescence molecular imaging with a radiative transfer model," *Molecular Imaging* 3(3), 230 (2004).
3. A.D. Klose, V. Ntziachristos, and A.H. Hielscher, "The inverse source problem based on the radiative transfer equation in optical molecular imaging," *J. Comp. Phys* 202, 323–345 (2005).
4. A. D. Klose and A. H. Hielscher, "Fluorescence tomography with simulated data based on the equation of radiative transfer," *Opt. Lett.* 28(12), 1019–1021 (2003).